VSPAERO Validation Case Studies

José Alfredo Rosas Córdova*

13 July 2022

Abstract

A series of validation case studies are carried out centered around the use of the VSPAERO vortex-lattice method solver integrated into OpenVSP. The results obtained with this tool are compared to reference values obtained by empirical relations, other similar aerodynamic solvers, and experimental measurements. A series of recommendations are given with regards to the meshing parameters, acceptable geometries, and valid flow conditions.

1 Introduction

VSPAERO is ~~a linear aerodynamic software packaged within the~~ NASA-developed OpenVSP parametric geometry tool [1]. The solver is ~~capable of utilizing the modelled geometry~~ to ~~predict~~ the aerodynamic characteristics using both vortex-lattice and panel methods. Alongside the possibility to study simple lifting surfaces such as aircraft wings and stabilizers, VSPAERO allows for the inclusion of propulsive elements and control surfaces ~~to carry out more complex analyses~~. The combination of a modelling tool specifically ~~design~~ for aircraft components alongside the ease of use of the VSPAERO solver has ~~resulted~~ in a set of software tools ~~of great use~~ during the early stages of aircraft conceptual design, where approximate solutions obtained by means of simplified methods suffice to determine whether or not an aircraft concept warrants further development.

~~As mentioned above, VSPAERO can be used to generated a series of different analyses important to aircraft design.~~ The basic use of the software is extremely simple: ~~one must only specified~~ the geometry to be analyzed and the pertinent flow conditions, after that running the software and getting results takes barely seconds with the simpler cases. ~~In this study only~~ the default vortex-lattice solver ~~is employed~~ as it is the easiest to set up and fastest to execute of the two available options. Some of the main tasks that can be accomplished using this solver are:

*Undergraduate Student, Centro de Investigación e Innovación en Ingeniería Aeronáutica, Universidad Autónoma de Nuevo León (CIIIA-UANL), jose.rosascdv@uanl.edu.mx

- aircraft polar plots;
- span-wise distribution plots;
- aerodynamic-propulsive analyses;
- stability analyses;
- control effectiveness analyses.

For a more in depth treatment on how to use the solver and the different output files for further analysis work, see [2].

Due to the relative novelty of this solver, not many validation studies have been published yet; two noteworthy exceptions can be found in [3], [4]. With the purpose of contributing to the wider use of this tool, as well to further the understanding ~~of the~~ usability of this solver ~~in problems of interest to the author~~, a series of validation studies ~~were carried out~~. The first five case studies ~~emanate from~~ [5], ~~where they were used to~~ validate the results of similar vortex-lattice solver, the considered selection encompasses analytical, hand-book based, and experimental reference results to compare against the values obtained using VSPAERO. The last two examples have the purpose of verifying the accuracy of the solver for use in designing small aircraft ~~immersed in flows of~~ low Reynolds numbers, the experimental data is obtained from [6].

Heavy use of the OpenVSP AngelScript and Python APIs allowed for the automation of all case studies, all the employed code is freely available in [7].

2 Validation Case Studies

Based on the results and recommendations given in [4], the tessellation parameters summarized in Table 1 were kept constant for all the performed analyses.

Parameter	Value
Leading edge cluster	0.25
Trailing edge cluster	0.25
Root cluster	1.0
Tip cluster	0.5

Table 1: Chord- and span-wise tessellation cluster parameters.

2.1 3D Properties of Two Wings

The first set of analyses was centered around determining the the best combination of chord- and span-wise mesh resolution to obtain good results within a reasonable execu-

tion time. Within OpenVSP the fineness of the mesh can be adjusted by modifying the tessellation values in the W and U directions, respectively.

The flow around two wings only differing in leading edge sweep was simulated at an angle of attack of 10°. The tessellation value was modified first along the chord-wise direction while maintaining the span-wise resolution to the default value of 6; afterwards, the span-wise tessellation was varied while the chord-wise value was kept constant at 33. The wing geometries can be seen in Fig. 1, their characteristics as well as the specified simulation parameters are summarized in Table 2.

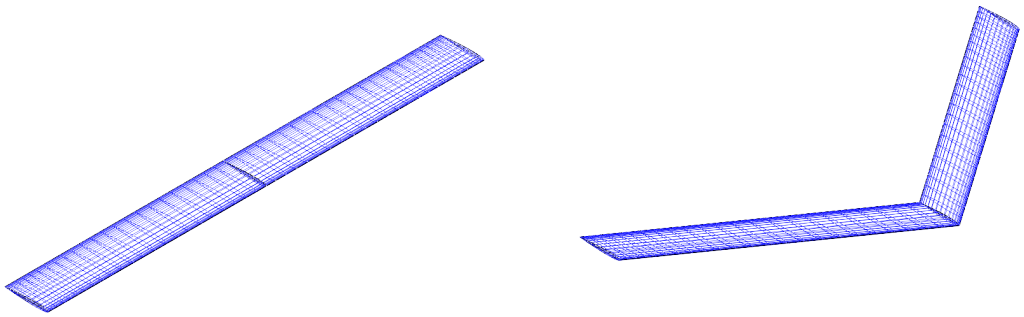

(a) (b)

Figure 1: Wings with (a) 0° and (b) 35° sweep angles used for the validation study.

Parameter	**Wing 1**	**Wing 2**
Span	10 ft	—
Chord	1 ft	—
Aspect ratio	10	—
Leading edge sweep	0°	35°
Airfoil	NACA 0009	—
Angle of attack	10°	—
Mach number	0.151	—
Chord-wise tessellation range	5 to 133	—
Span-wise tessellation range	6 to 54	—

Table 2: Geometric and simulation parameters employed in the test case study.

The results obtained by carry out the previously described tests are shown in Figs. 2 and 3. The VSPAERO data points are plotted along side the reference value and the results given by the SURFACES vortex-lattice solver. The shaded region represents the $\pm 5\,\%$ error band with respect to the reference value.

For this case study, the reference values emanate from the empirical relations given in the USAF DATCOM. The relations used in [5] are repeated here for convenience[1] are

$$C_{L_\alpha} = \frac{2\pi \cdot AR}{2 + \sqrt{\left(\frac{AR \cdot c_{L_\alpha}}{2\pi}\right)^2 \left(1 + \frac{\tan \Lambda_{c/2}{}^2}{1 - Ma^2}\right)} + 4}; \tag{1}$$

$$C_{D_i} = \frac{C_L^2}{\pi \cdot AR}; \tag{2}$$

with

$$C_{L_0} = 0. \tag{3}$$

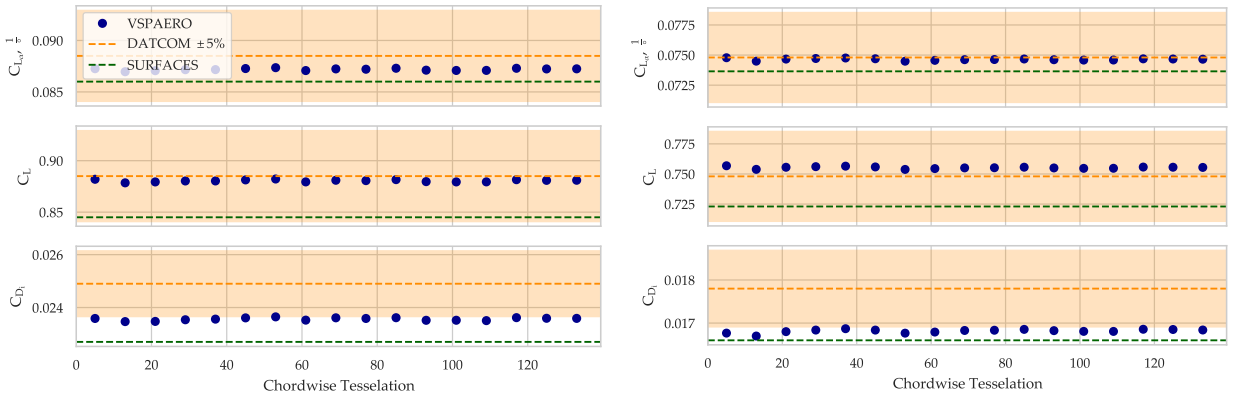

(a) (b)

Figure 2: Results obtained by modifying the wing chord-wise tessellation value for the (a) 0° and (b) 35° sweep wings.

The chord-wise tessellation has a almost unnoticeable effect on the obtained results. Even though the studied range was considerably large, the percent difference between the first and last points for all six plots averages at 0.030 %. In a similar manner, the solution times of the coarsest and finest mesh are practically the same. On the other hand, the effect of the span-wise tessellation had a more noticeable effect on both the accuracy of the results as well as the simulation execution time. Starting from the minimum allowable tessellation value of 2, the coefficient values converge rather quickly. While for the straight wing any tessellation value after the second point, around the 4 mark, would yield an appropriate result; the swept wing needs a significantly finer mesh to be able to yield consistent results. The use of an excessively refined mesh along the span-wise direction is limited by the fact that above a value of 30 the simulation times start to increase significantly.

[1]The computations employed to reach the final values are carried out in full detail in [5] but are omitted here for the sake of brevity.

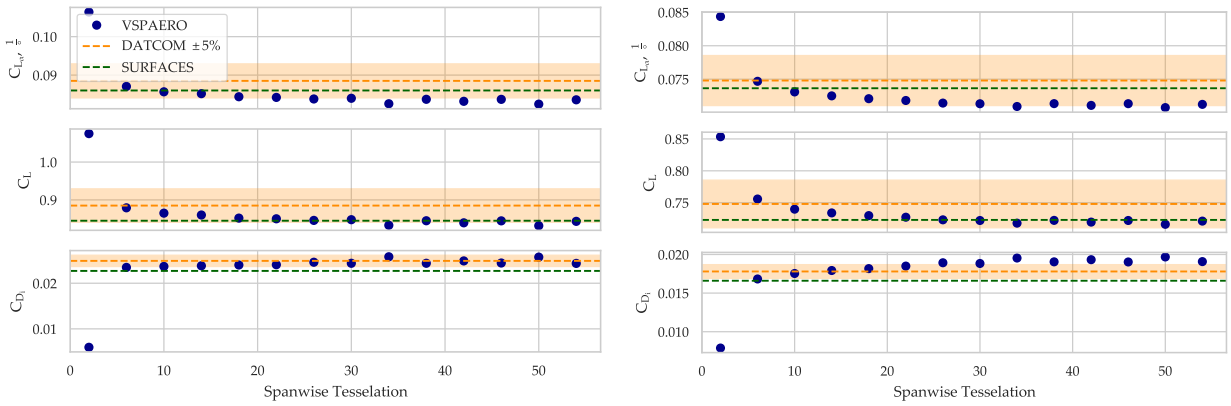

(a) (b)

Figure 3: Results obtained by modifying the wing span-wise tessellation value for the (a) 0° and (b) 35° sweep wings.

From the obtained results it was determined that a wing with a chord- and span-wise tessellation values of 33 and 24, respectively, would provide adequate results in a reasonable amount of time. This tessellation settings were employed in the rest of the analyses described in this document. Table 3 compares the results using these tessellation settings to the reference values for the two studied wing geometries.

	Wing 1			Wing 2		
Coefficient	**DATCOM**	**VSPAERO**	**Error, %**	**DATCOM**	**VSPAERO**	**Error, %**
C_{L_α}, rad^{-1}	5.071	4.824	4.81	4.286	4.108	4.10
C_L	0.885	0.851	3.89	0.748	0.726	2.92
C_{D_i}	0.0249	0.0239	3.85	0.0178	0.0185	4.03

Table 3: Comparison of the VSPAERO and DATCOM reference results for both wings with a chord- and span-wise tessellation values of 33 and 24, respectively.

2.2 Warren-12 Wing

The Warren-12 wing model is a standard case study for the validation of new or modified VLM codes [5]. The published planform geometry and aerodynamic characteristics of the wing are compiled in Table 4, the OpenVSP model is shown in Fig. 4.

As mentioned in the previous section, the wing tessellation was set to 33 and 24 for the chord- and span-wise directions, respectively. An angle of attack sweep from 0° to 10° was simulated with VSPAERO and the results were plotted against the reference values reported in [5]. Figure 5 shows the resulting lift a pitching moment coefficient plots.

Parameter	Value
Span	2.83 ft
Root chord	1.50 ft
Tip chord	0.50 ft
Aspect ratio	2.83
Leading edge sweep	53.54°
$C_{L_\alpha}{}^{*}$	2.743 rad^{-1}
$C_{M_\alpha}{}^{\dagger}$	−3.10 rad^{-1}

$^{*}\, c_{ref} = 1\,\text{ft}; \quad ^{\dagger}\, x_{CG} = 0\,\text{ft}.$

Table 4: Published geometric and aerodynamic characteristics of the Warren-12 wing.

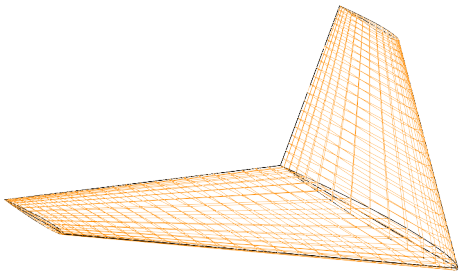

Figure 4: Warren-12 wing modelled in OpenVSP.

Although expected, the agreement between the three curves shown in Fig. 5 is still remarkable. The values of the obtained coefficient derivatives as well as the average percent error with respect to the reference value of the points calculated with VSPAERO and the ones obtained using SURFACES reported in [5] are summarized in Table 5.

		VSPAERO		SURFACES	
Coefficient	**Published Data**	**Value**	**Error, %**	**Value**	**Error, %**
C_{L_α}, rad^{-1}	2.715	2.743	1.01	2.767	1.92
C_{M_α}, rad^{-1}	-3.020	-3.10	2.56	-3.139	3.94

Table 5: Comparison of the VSPAERO, SURFACES, and published reference results for the Warren-12 wing.

Similarly to the previous results, the average percent error does not exceed the 5 % mark, an outstanding result for a solver that allows for such quick computations as VS-

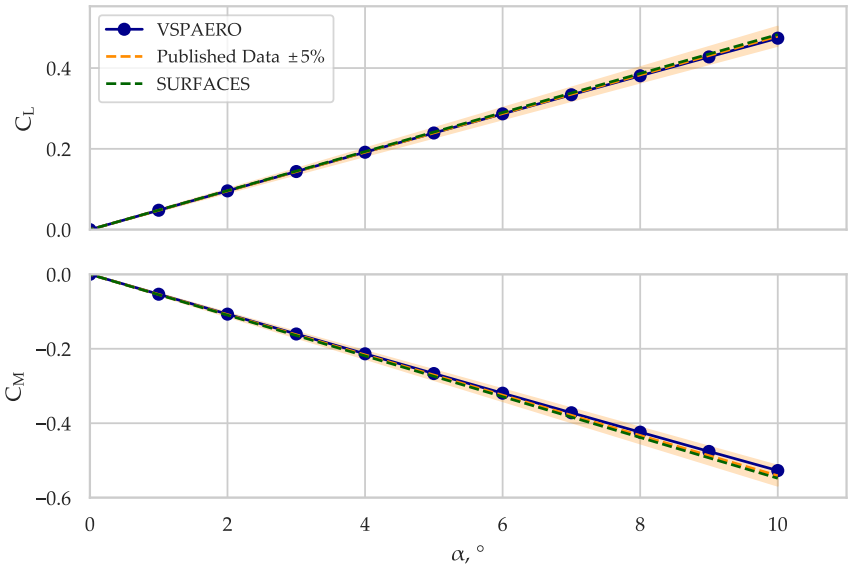

Figure 5: Calculated and reference lift and pitching moment coefficient curves of the Warren-12 wing.

PAERO.

2.3 Bertin-Smith 2D Wing

Similarly to the previous case, the Bertin-Smith 2D wing is a specified known geometry with known results. The wing is given out as an exercise in [8], here a series of calculations are carried out to determine the value of the lift curve slope. Table 6 summarizes the geometry of the wing as well as the calculated lift curve slope obtained in the book. Figure 6 shows the wing geometry modelled in OpenVSP.

Parameter	**Value**
Span	1.0 ft
Chord	0.20 ft
Aspect ratio	5.0
Leading edge sweep	45°
$C_{L_\alpha}{}^*$	3.433 rad^{-1}

* At $\alpha = 0°$.

Table 6: Geometric and aerodynamic characteristics of the Bertin-Smith wing.

Analogous to the procedure followed in Section 2.2,the chord- and span-wise tessellations were set to 33 and 24, respectively. A sweep VSPAERO analysis from 0° to 10°

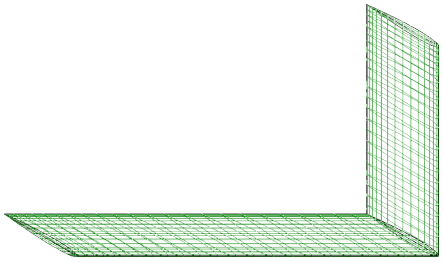

Figure 6: Wing geometry modelled in OpenVSP.

was carried out resulting in the curve shown in Fig. 7. Alongside the lift curve calculated with VSPAERO, the plot also includes the reference slope reported in [8] and two other curves computed using two alternative VLM solvers: SURFACES and Tornado [5]. Table 7 summarizes the obtained results for the three solvers.

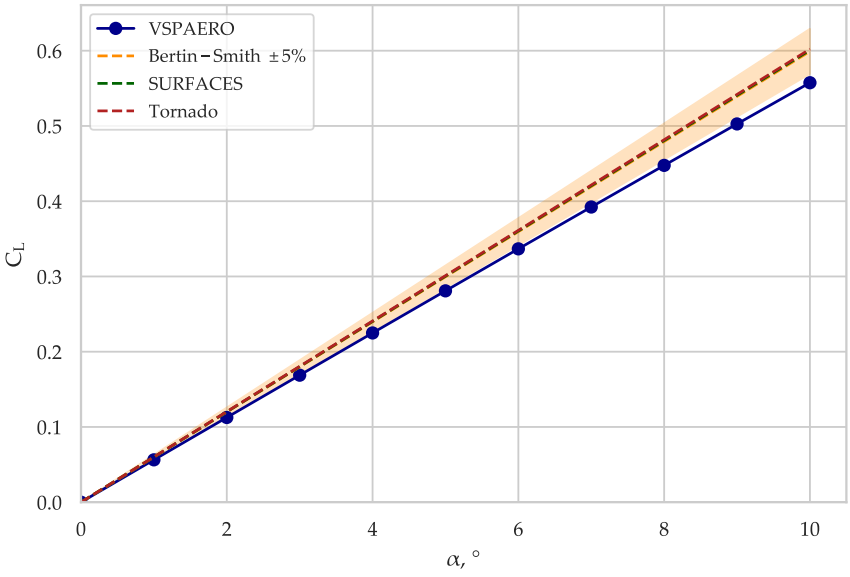

Figure 7: Lift curve for the Bertin-Smith wing calculated with different methods.

For this case, the results obtained by using VSPAERO are significantly less accurate than the ones obtained from the other two solvers. The tendency of the solver to underpredict the value of the lift curve slope can be also identified in Fig. 3. Despite the above, taking into account that this deviation only amounts to approximately 7 % of the original value, the results can still be considered adequate for the early stages of the design process.

		VSPAERO		SURFACES		Tornado	
Coefficient	**Bertin-Smith**	**Value**	**Error, %**	**Value**	**Error, %**	**Value**	**Error, %**
C_{L_α}, rad^{-1}	3.433	3.194	6.96	3.442	0.26	3.450	0.50

Table 7: Comparison of the VSPAERO, SURFACES, Tornado, and the calculated reference value reported in [8].

2.4 NACA R-1208

In contrast to the previously considered analyses, this case study uses experimental values as a reference to measure the accuracy of the VSPAERO results, specifically the wind-tunnel measurements carried out in [9]. Similarly to previous cases, the wing geometry is a swept-back wing of moderate aspect ration. The main geometric characteristic of the wing are compiled in Table 8, while the generated OpenVSP goemtry is shown in Fig. 8.

Parameter	**Value**
Span	10.605 ft
Root chord	1.828 ft
Tip chord	0.823 ft
Aspect ratio	8.0
Quarter chord sweep	45°
Airfoil	NACA 63_1A012

Table 8: Geometric parameters of the wing studied in [9].

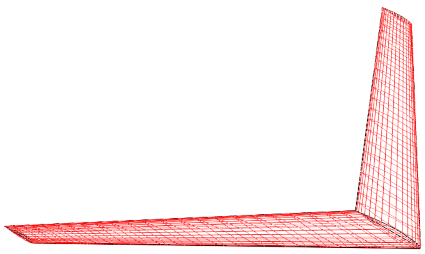

Figure 8: NACA R-1208 wing geometry modelled in OpenVSP.

Based on the available experimental data in [9], the two follwoing analyses were carried out:

1. An angle of attack sweep from 0° to 10° to get the lift and pitching moment coefficient curves of the wing.
2. A load distribution analysis at a fixed angle of attack of 4.7° to obtain the normalized lift coefficient distribution along the span of the wing.

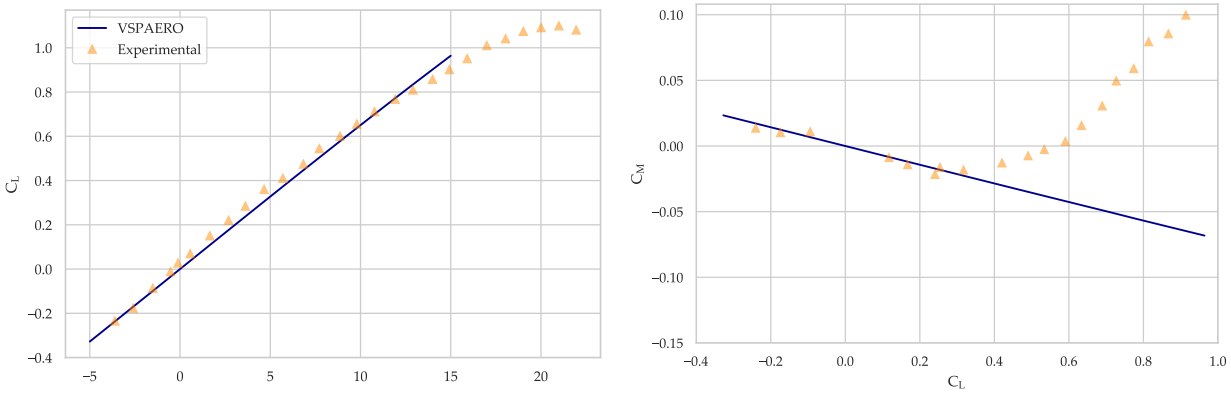

(a) (b)

Figure 9: Resulting (a) lift and (b) pitching moment coefficient curves plotted against data points obtained experimentally.

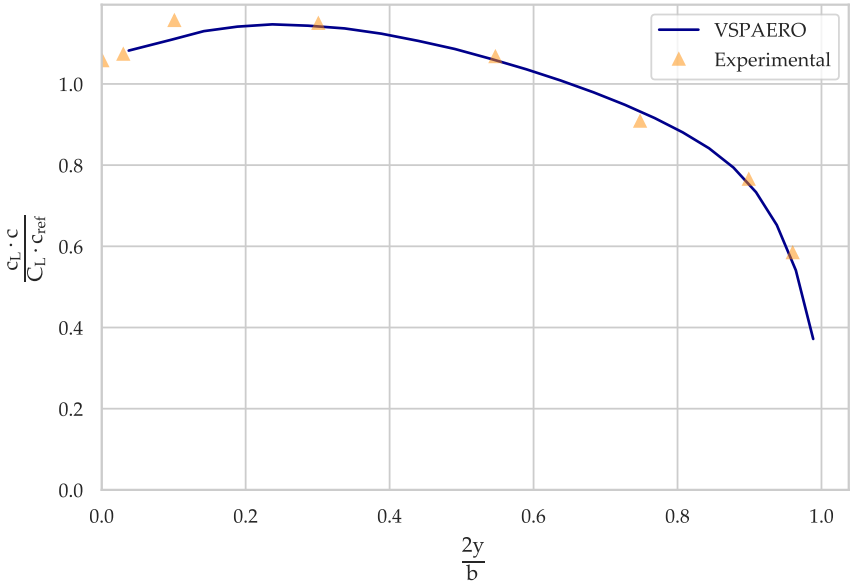

Figure 10: Normalised span-wise lift coefficient distribution obtained from both VSPAERO and experimental analyses.

The part of the analyses centered around determining the lift and pitching moment curves the resulting plots are shown in Fig. 9. The lift curve shows good agreement with

the experimental values throughout the linear range. On the other hand, the calculated moment coefficient values on the second half of the studied range deviate significantly from the expected experimental values, this can be explained with the early tip stall phenomena characteristic of swept back wings, something impossible to predict for a inviscid solver; a similar result is obtained in [5] with the SURFACES VLM solver. In the case of the local lift coefficient distribution, the results computed using VSPAERO shows close agreement to the reported experimental values. Table 9 summarizes the obtained results for this case study.

Coefficient	R-1208	VSPAERO	Error, %
C_{L_α}, rad^{-1}	3.493	3.700	5.91
$\frac{dC_M}{dC_L}$*	-0.0727	-0.0714	1.59
$c_L = f\left(\frac{2y}{b}\right)$	—	—	2.50

* Before tip stall.

Table 9: Comparison between the results obtained from VSPAERO and the experimental findings reported in [9].

2.5 NACA TN-1422

This case study is based in the wind-tunnel test results reported in [10] for two wings only differing in the washout angle. The employed wing geometry is that of a straight tapered wing of moderate aspect ratio, the parameters of which are presented in Table 10. The general wing planform can be seen in Fig. 11.

Parameter	Wing 1	Wing 2
Span	15.0 ft	—
Root chord	21.381 ft	—
Tip chord	0.952 ft	—
Aspect ratio	9.0	—
Quarter chord sweep	0.0°	—
Dihedral	3.0°	—
Washout	0.0°	2.0°
Airfoil	NACA 65-210	—

Table 10: Geometric characteristics of the wings tested in [9].

Analogous to the previous section, VSPAERO was employed to carry out an angle of attack sweep as well as a span-wise lift coefficient distribution for the two lifting surfaces; the obtained results where then plotted against the reported experimental values. Both

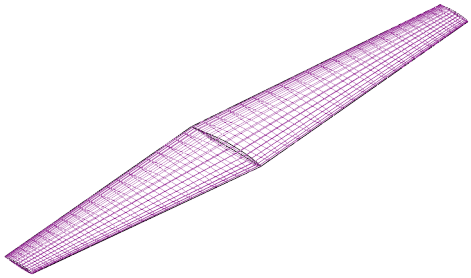

Figure 11: NACA TN-1422 wing geometry modelled in OpenVSP.

calculated and experimental lift and pitching moment coefficient curves for both washout cases can be seen in Fig. 12; similarly, the span-wise lift coefficient distributions are shown in Fig. 13.

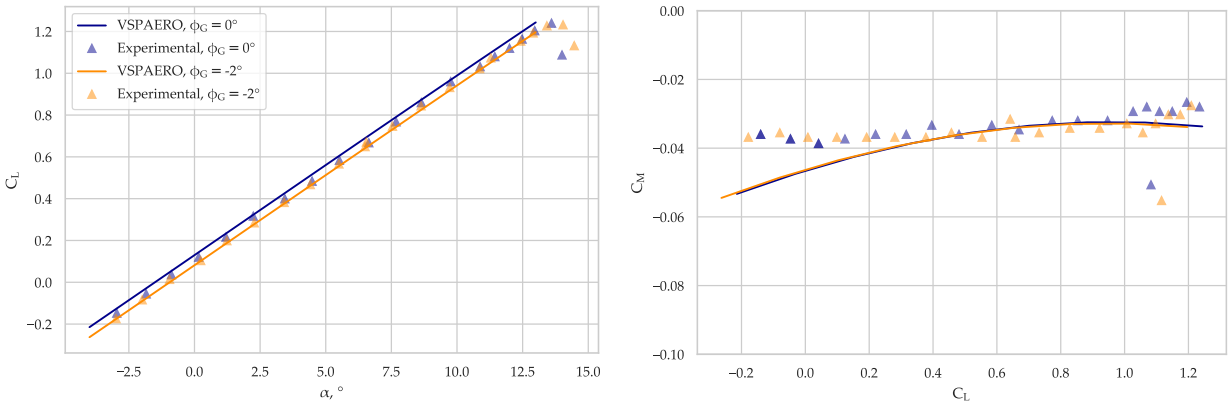

(a) (b)

Figure 12: Calculated (a) lift and (b) pitching moment coefficient curves plotted against data points obtained experimentally for the two tested wings at stall.

In the same manner as the results of Section 2.4, the calculated lift curves follow the experimental points exceptionally well. The pitching moment coefficient curve loses accuracy at the extremes of the studied range, this combined with the close to zero values of the slope yields high percent error values for the relatively small absoulute differences. Finally, the span-wise lift coefficient distribution show good agreement in both cases. A summary of the obtained values can be seen in Table 11.

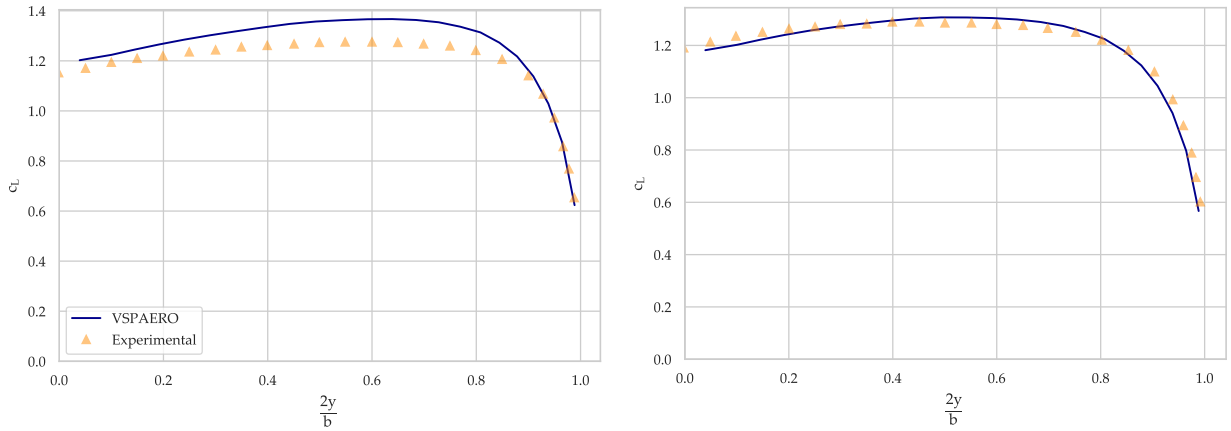

(a) (b)

Figure 13: Calculated and experimentally determioed span-wise local lift coefficient distribution obtained for (a) Wing 1 and (b) Wing 2.

	Wing 1			Wing 2		
Coefficient	**TN-1442**	**VSPAERO**	**Error, %**	**TN-1442**	**VSPAERO**	**Error, %**
C_{L_α}, rad^{-1}	4.850	4.915	1.34	4.938	4.920	0.38
$\frac{dC_M}{dC_L}$	0.0071	0.0128	81.69	0.0059	0.0121	106.12
$c_L = f\left(\frac{2y}{b}\right)$	—	—	4.80	—	—	2.26

Table 11: Comparison between the results obtained from VSPAERO and the experimental findings reported in [10].

2.6 Low-Re Wings of Different Aspect Ratios

The potential to apply VSPAERO to aid the design of small aircraft is a topic of special interest to the author. In order to validate the applicability of the solver to wings at low Reynolds number flows these last two case studies make use of the wind tunnel test results reported in [6] as reference values to compare against the calculated values.

For this case study, the lift curve of a set of rectangular wings of our different aspect ratios were calculated and compared with experimentally determined values. The reference values correspond to wind-tunnel tests with $Re = 100,000$. Table 14 summarizes the geometry of the analyzed wings. The OpenVSP models of the four wings are shown in Fig. 14.

The calculated lift curve plots for the four wings alongside the experimentally determined points are shown in Fig. 15. From the resulting image it becomes clear that the solver has a tendency to under-predict the lift curve slope for the wings of the smallest aspect ratio, similarly to the deviation seen in Fig. 9b, this can be attributed to either vis-

Parameter	Wing 1	Wing 2	Wing 3	Wing 4
Span	0.583 ft	0.875 ft	1.167 ft	1.458 ft
Chord	0.292 ft	—	—	—
Aspect ratio	2.0	3.0	4.0	5.0

Table 12: Geometric characteristics of the four tested wings.

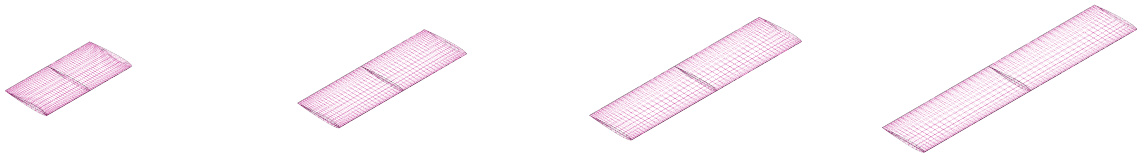

(a) (b) (c) (d)

Figure 14: Wings with aspect ratio values of (a) 2.0, (b) 3.0, (c) 4.0, and (d) 5 modelled in OpenVSP.

cous or out-of-plane aerodynamic effects (e.g. vortex lift) that are not considered by the VLM solver. The obtained lift curve slope and percent error results are summarized in Table 13, while the two wings with smaller aspect ratio show significant deviations from the experimentally determined values, the two wings of higher AR show good agreement between the two values.

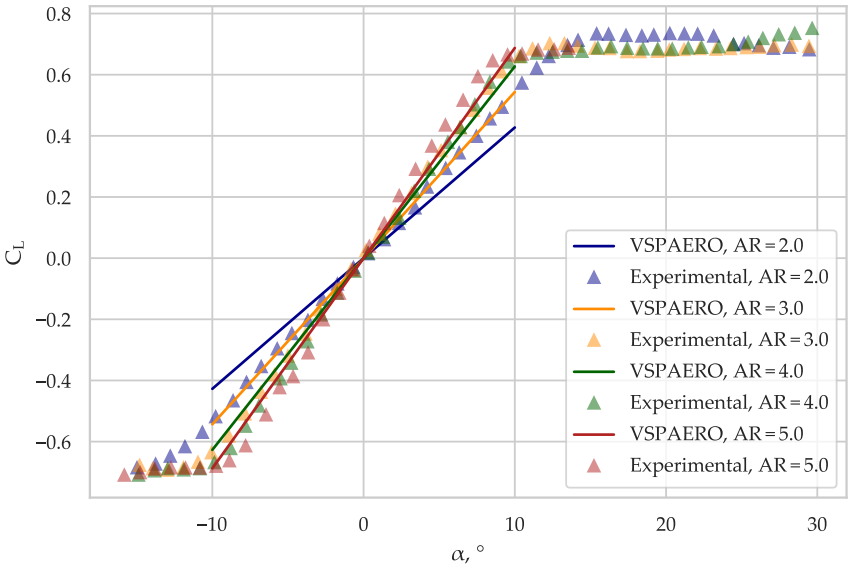

Figure 15: Calculated and experimentally determined lift curves for the four tested wings.

Aspect Ratio	Experimental, rad^{-1}	VSPAERO, rad^{-1}	Error, %
2.0	3.0814	2.4483	20.55
3.0	3.6697	3.1137	15.15
4.0	3.7876	3.5926	5.15
5.0	3.8615	3.9388	2.00

Table 13: Comparison between the VSPAERO and experimental results for the four analyzed wing geometries.

2.7 Low-Re Wings of Different Taper Ratios

Analogous to the previous section, this case study contemplates a set of small wings of different taper ratio also in a flow with $Re = 100,000$. The geometric parameters of the three analyzed wings are compiled in Table 15, Fig. 16 shows the corresponding OpenVSP models.

Parameter	Wing 1	Wing 2	Wing 3
Span	1.125 ft	1.159 ft	1.167 ft
Root chord	0.375 ft	0.331 ft	0.292 ft
Taper ratio	0.50	0.75	1.00
Aspect ratio	4.0	—	—

Table 14: Geometric parameters of the three tested wings.

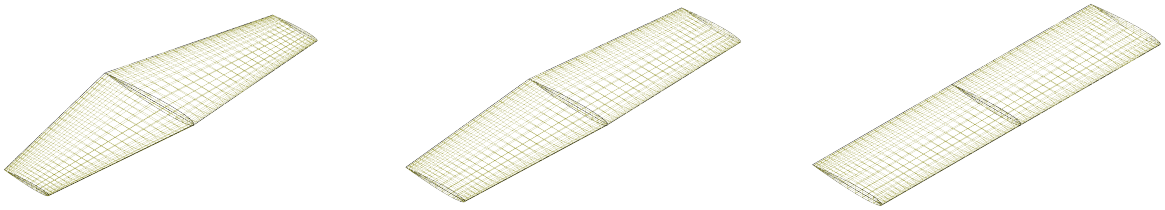

(a) (b) (c)

Figure 16: Wings with taper ratio values of (a) 0.50, (b) 0.75, and (c) 1.00 modelled in OpenVSP.

Figure 17 shows the three lift curves calculated using VSPAERO plotted on top of the experimentally determined points. Similarly to the case of the wings with higher aspect ratio analyzed in Section 3.2, the calculated lift curves follow the experimental data points in a relatively precise manner; this may be a by product of all the studied wings having an aspect ratio of 4.0, the minimum value that yielded good results in the previous validation

case. The lift curve slope and error values resulting from the analyses are compiled in Table 15.

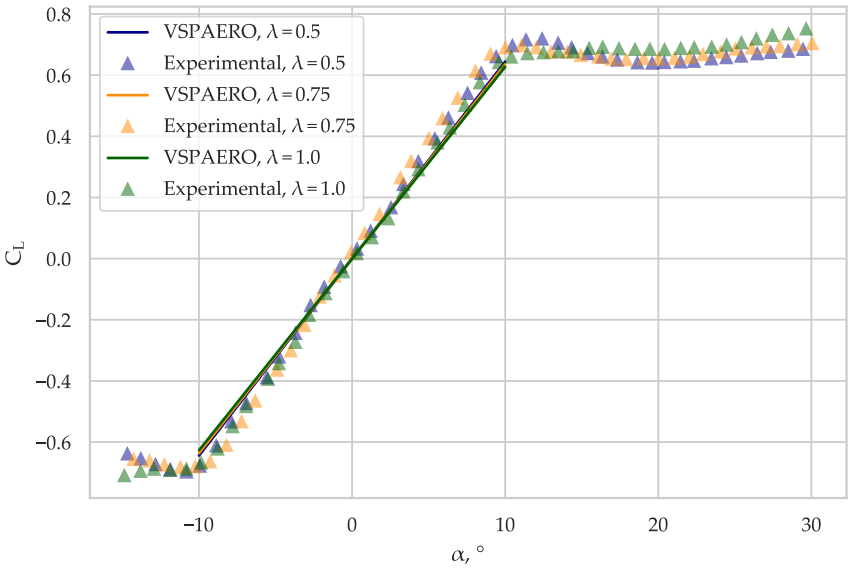

Figure 17: Calculated and experimentally determined lift curves for the three tested wings.

Taper Ratio	Experimental, rad^{-1}	VSPAERO, rad^{-1}	Error, %
0.5	3.8971	3.6905	5.3
0.75	3.9128	3.6471	6.79
1.00	3.7876	3.5926	5.15

Table 15: Comparison between the VSPAERO and experimental results for the three studied wing geometries.

3 Discussion

3.1 Wing Tessellation

The tests carried out in Section 2.1 shed light on the effects a coarser or finer mesh had on the obtained results, these results were then employed to define a standard set of tessellation parameters for the rest of the case studies (i.e. a chord- and span- wise tessellation values of 33 and 24, respectively). The relatively accurate results obtained in the remaining case studies confirmed that the employed tessellation parameters are adequate values for carrying out VSPAERO calculations.

3.2 Lift Curve and Distribution Calculation

With the exception of the first two wings tested in , all lift curve slope and distribution calculations provided accurate results well within the $\pm 5\,\%$ band of the corresponding reference values. The fact that this applies for both handbook, theoretical, and experimental values as well as for different flow regimes proves the value of VSPAERO as a aerodynamic prediction tool. This is only the case, however, if the limitation of the solver are taken into account, mainly:

- The resulting lift curve is limited to the linear region where viscous characteristics are mostly confined in the boundary layer.
- The incapability of the solver to give accurate results for particular geometries, for example, highly swept wings at moderate angles of attack or low aspect ration wings.

3.3 Moment Curve Calculation

Analogous to the lift calculations, the VSPAERO results obtained in the distinct case studies proved of adequate accuracy when the limitation of the VLM linear solver are taken into account. Special attention must be given to highly swept wings, where a accurate lift prediction may not correspond to a accurate pitching moment result.

3.4 Effects of Wing Geometric Parameters

As already mentioned, the linear nature of the solver imposes some limitations on the geometries and flow conditions that may be analyzed if relatively accurate results are to be expected. On this matter, the following can be summarized:

- The analysis of wings with an aspect ratio less than 4.0 seems to yield overly-pessimistic results when compared with the corresponding reference values[2], once this minimum is surpassed, the percent error margins are significantly reduced.
- The study of highly swept wings were a span-wise flow component can lead to early tip-stalling must be kept within a conservative angle of attack range if good lift and moment predictions are desired.
- Ordinary taper ratio variations did not seem to have a significant effect on the accuracy of the results given the other geometric considerations are kept in mind.

[2]The case study presented in Section 2.2 uses reference values based on theoretical calculation, this is the reason the deviations are not as large despite the low aspect ratio of the wing geometry.

4 Conclusion

The results obtained from this collection of case study validate the applicability of VSPAERO as an aerodynamic analysis tool for the estimation of, among others, lift and moment characteristics of an aircraft during the conceptual phase of its development. A more nuanced use of the tool can lead to overall more accurate results, this can be achieved by employing the recommended meshing parameters as well as by understanding the uncovered software limitations related to both wing geometry and flow conditions.

Future work should focus on validating some of the other analysis available in VSPAERO. In the context of small electric aircraft design, special interest is to be given to both the aerodynamic-propulsive analysis possibilities and the tools for stability characterization.

References

[1] "OpenVSP," National Aeronautics and Space Administration. (2012), [Online]. Available: http://openvsp.org (visited on 07/09/2022).

[2] B. Litherland. "Using VSPAERO," National Aeronautics and Space Administration. (2015), [Online]. Available: http://openvsp.org/wiki/doku.php?id=vspaerotutorial (visited on 07/09/2022).

[3] L. Payne, "VSPAERO Verification Testing," in *OpenVSP Workshop 2017*, Empirical Systems Aerospace, Inc., 2017. [Online]. Available: http://openvsp.org/wiki/lib/exe/fetch.php?media=workshop17:payne-vspaero_verification.pdf.

[4] F. Mariën, "Software Testing: VSPAERO," M.Sc. thesis, Hamburg University of Applied Science, 2021.

[5] *SURFACES - User Manual - Vortex-Lattice Module*, Great OWL Publishing, 2009.

[6] G. K. Ananda Krishnan, "Aerodynamic Performance of Low-to-Moderate Aspect Ratio Wings at Low Reynolds Numbers," M.Sc. thesis, University of Illinois at Urbana-Champaign, 2012.

[7] J. A. Rosas Córdova. "vspaero-validation-studies." (2022), [Online]. Available: https://github.com/JARC99/vspaero-validation-studies (visited on 07/12/2022).

[8] J. J. Bertin and R. M. Cummings, *Aerodynamics for Engineers*, 6th ed. Upper Saddle River, NJ: Pearson, 2013.

[9] W. C. Schneider, "A Comparison of the Spanwise Loading Calculated by Various Methods with Experimental Loadings Obtained on a 45° Sweptback Wing of Aspect Ratio 8.02 at Reynolds 4.0×10^6," Report 1208, 1951.

[10] J. C. Sivells, "Experimental and Calculated Characteristics of Three Wings of NACA 64-210 and 65-210 Airfoil Sections with and without 2° Washout," Technical Note No. 1422, 1947.